Hybrid organic–inorganic layered TiO2 based nanocomposite for sunlight photocatalysis

ARTICLE *in* RSC ADVANCES · FEBRUARY 2016

Impact Factor: 3.84 · DOI: 10.1039/C5RA26981D

7 AUTHORS, INCLUDING:

Eglantina Benavente

Universidad Tecnológica Metropolitana

68 PUBLICATIONS **848** CITATIONS

SEE PROFILE

Harold Lozano-Zarto

University of Chile

11 PUBLICATIONS **23** CITATIONS

SEE PROFILE

Clivia M. Sotomayor Torres

Catalan Institute of Nanoscience and Nano…

488 PUBLICATIONS **6,525** CITATIONS

SEE PROFILE

RSC Advances

COMMUNICATION

Cite this: *RSC Adv.*, 2016, **6**, 18538

Received 17th December 2015
Accepted 5th February 2016

DOI: 10.1039/c5ra26981d

www.rsc.org/advances

A hybrid organic–inorganic layered TiO_2 based nanocomposite for sunlight photocatalysis†

Eglantina Benavente,*[ae] Carlos Maldonado,[ae] Sindy Devis,[be] Leslie Diaz,[ce] Harold Lozano,[be] Clivia Sotomayor-Torres[d] and Guillermo González[be]

A novel hybrid nanocomposite constituted of single TiO_2 nanosheets sandwiched between stearic acid self-assembled monolayers was synthesized and tested in the photodegradation of methylene blue under sunlight. The product showed better photocatalytic performance than anatase under similar conditions, which may be further improved through sensitization with cadmium sulfide.

Introduction

Wide-bandgap semiconductors such as TiO_2, ZnO, and SnO_2 have received much attention because of their promising applications in waste-water purification, as well as solar energy conversion.[1–4] Nanostructured TiO_2-based photocatalysts remain the most promising materials owing to their high photoactivity, physical and chemical stability, nontoxicity, and low cost.[5,6] However, restrictions like the fast recombination of photogenerated electrons/holes (e^-/h^+) and poor harvesting of visible light limit the use of TiO_2 in cost-effective environmental remediation processes. Numerous approaches to solve the drawbacks of TiO_2 have been reported.[7,8] Among them, the extension of TiO_2 absorption towards lower energies by creating electronic levels within its bandgap, for instance by doping TiO_2 with metal or non-metal species[9–14] and, very recently, by coating the crystalline stoichiometric TiO_2 with a shell rich in defects of amorphous black TiO_2.[15,16] TiO_2 sensitization with dyes or other semiconductors has been also widely used.[6–8,17–19] Improved photocatalysts have been obtained by the coupling of CdS with low-dimensional nanostructures of TiO_2 tubes, rods, wires or nanosheets,[20–23] possibly due to a reduced photoinduced charge carrier recombination rate, promoted by the higher aspect ratio of the particles. The photocatalyst capability for adsorbing organic pollutants at its surface, though only rarely considered until now,[24] is also relevant for designing efficient catalysts.

This communication focuses on the photocatalytic behavior of a new organic–inorganic hybrid nanocomposite, TiO_2(stearic acid)$_{1.1}\cdot 0.6H_2O$ ($LHTiO_2$), where both the low dimensionality of TiO_2 and the adsorption ability of the organic component are conjugated. The photoactivity of this nanocomposite, both as-prepared and sensitized by CdS, was tested regarding the degradation of aqueous methylene blue (MB) under sunlight. The results were clearly improved with respect to that of anatase under similar conditions.

The $LHTiO_2$ nanocomposite was prepared by the reaction of titanium tetraisopropoxide (TTIP) with stearic acid in ethanol. The SEM images of the product (Fig. 1A and B) reveal microstructured aggregates of particles with a lamellar morphology. The XRD pattern of the product (Fig. 2A) corroborates the lamellar nature of the nanocomposite. The diffraction peaks at 2θ values of 2.98°, 6.10° and 9.17° are in good agreement with the three first (00l) reflections in a lamellar solid with a basal-distance along the c-axis of 29.6 Å. The low intensity peaks at 20.21° and 21.39° may be ascribed to a small excess of free stearic acid (JCPDS 03-0252). The average thickness of the nanosheets, 18 nm, was estimated by the Scherrer equation and approximately corresponds to six single sheets of the hybrid per particle.[25] The Raman spectrum of as-prepared $LHTiO_2$ (Fig. 2C), did indicate the product was defect-rich and poorly crystalline. Spite of that, the more prominent features in the spectrum could be assigned to several of the vibration modes reported for the TiO_2(B)[26] (arrows in Fig. 2C). In turn, the spectra of TiO_2 samples calcined at 185 and 500 °C (Fig. S1†) showed that the TiO_2(B) phase was thermally instable. The spectrum of the sample calcined at 185 °C corresponded to a completely amorphous material; no peak of any stable TiO_2 phases was apparent; and only some few features from residual carboxylic

[a]*Universidad Tecnológica Metropolitana, P.O. Box 9845, Santiago, Chile. E-mail: ebenaven@utem.cl; Tel: +56-227877109*

[b]*Universidad de Chile, P.O. Box 653, Santiago, Chile*

[c]*Universidad de Santiago de Chile, P.O. Box 10233, Santiago, Chile*

[d]*Catalan Institute of Nanotechnology (CIN2-CSIC) Campus Bellaterra, Spain*

[e]*Center for the Development of Nanocience and Nanotechnology, CEDENNA, Santiago, Chile*

† Electronic supplementary information (ESI) available: Experimental section and additional characterization. See DOI: 10.1039/c5ra26981d

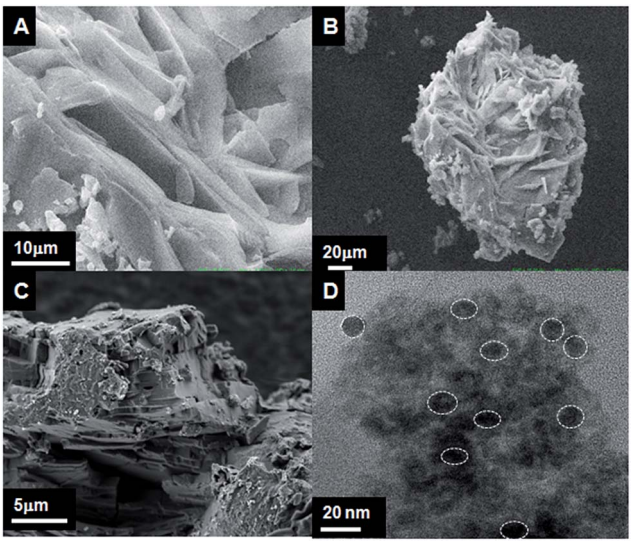

Fig. 1 SEM images of $LHTiO_2$ (A and B), SEM images of $LHTiO_2$/CdS0.05 (C) and TEM images of $LHTiO_2$/CdS0.05, CdS NPs featured in circles in the image (D).

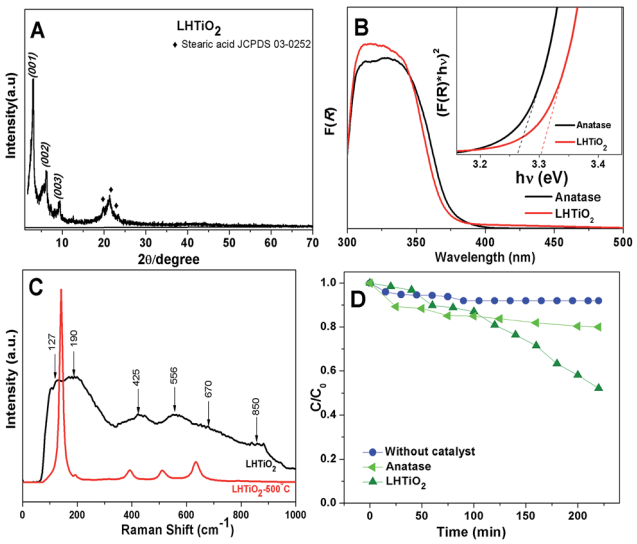

Fig. 2 XRD patterns of $LHTiO_2$ (A), UV-vis diffuse reflectance spectra of anatase and $LHTiO_2$, in insert, band gap are calculated according to Kubelka–Munck function (see ESI†) (B), Spectra Raman of $LiHTiO_2$ and $LiHTiO_2$ calcined at 500 °C (C), plots of the degradation of MB solution under sunlight without catalyst, in the presence of $LHTiO_2$ and of anatase (D).

acid (Fig. S1†) were identifiable. At 500 °C the $LHTiO_2$ became quantitatively into pure anatase.

Both elemental and thermogravimetric analysis (Fig. S2†) of the product indicate the formation of a commensurate nanocomposite $TiO_2(\text{stearic acid})_{1.1}\cdot 0.6H_2O$ ($LHTiO_2$), with a ~10% excess of free carboxylic acid. Fig. 2B shows the UV-vis diffuse-reflectance spectra of samples of as-prepared $LHTiO_2$ and TiO_2 anatase. The photoresponse of $LHTiO_2$ in the UV region is qualitatively similar to that of anatase. However, the band-edge in the spectrum of the nanocomposite (insert in Fig. 2B) was slightly blue-shifted, with respect to that of TiO_2, corresponding to an increase in the bandgap of about 0.1 eV, which could be ascribed to 2D confinement of the semiconductor. In order to identify the role of carboxylic acid in the nanocomposite, we analyzed the infrared spectrum of the product (Fig. S3†). The two bands at 1560 and 1315 cm^{-1}, corresponding to the asymmetric and symmetric ν(C–O) modes, respectively, demonstrate that the organic moiety is found as a carboxylate monocoordinated to the inorganic sheets.[27] The low intensity ν(C–O) band at 1705 cm^{-1} corroborates the presence of a small amount of free acid in the sample. According to the available evidence, the $LHTiO_2$ nanocomposite can be described as a two-phase nanostructure in which carboxylic acid is intercalated between inorganic sheets (Fig. S4†).

The photocatalytic performance of $LHTiO_2$ was tested for the photodegradation of methylene blue (MB) under sunlight, in aqueous solution and ambient conditions. The photocatalytic efficiency of $LHTiO_2$ after 220 min irradiation, about 49%, was significantly higher than that of anatase under similar conditions, *i.e.* about 20% (Fig. 2D); this occurred in spite of the slightly larger band gap of $LHTiO_2$. The increased photoactivity of $LHTiO_2$ under visible light could be caused by the almost imperceptible extent of its absorption band (Fig. 2B and S5†). This effect appears to correspond to the Urbach tail which has been explained by the creation of discrete electronic levels inside the TiO_2 band gap (Fig. S6†).[28,29]

To further investigate the photocatalytic behavior of $LHTiO_2$, CdS-sensitized $LHTiO_2$ was fabricated using cadmium sulfide nanoparticles (CdS NPs) (JCPDS 10-0454, Fig. S7†). Four composite samples containing 0.1, 0.05, 0.025, and 0.0125 moles of CdS per mole of titanium oxide were prepared by mixing the components under sonication. SEM images (Fig. 1C) revealed that the lamellar nature of the precursor $LHTiO_2$ was retained in the composites. No changes were observed in DRX after adding CdS, probably due to the low concentration (<5%) of the latter. The TEM image of the $LHTiO_2$/CdS 1 : 0.05 sample showed CdS NPs ~10–18 nm in size, featured in circles in the image (Fig. 1D). The EDX spectrum (Fig. S8†) corroborated the presence of cadmium and sulfur in the sample. The UV-vis-diffuse reflectance spectra (Fig. 3A) showed that the absorption edge at 373 nm in the $LHTiO_2$ was extended to ~575 nm in the composite. The photocatalytic properties of as-prepared CdS/$LHTiO_2$ composites were evaluated under conditions similar to those used for $LHTiO_2$ (MB concentration, sunlight, room temperature). Among the tested samples, the one with 0.05 moles of CdS per mole of titanium showed the highest photocatalytic efficiency (Fig. S9†). The comparison of catalytic activity of this sample with those of its components $LHTiO_2$ and CdS NPs and with anatase (Fig. 3A) indicated that, after 220 min of sunlight irradiation, 20%, 49%, 67%, and 90% of MB was degraded when using anatase, $LHTiO_2$, CdS NPs, and the $LHTiO_2$/CdS composite, respectively. The apparent rate constants (k_{app}, min^{-1}) for $LHTiO_2$/CdS were about 5 and 6 times faster than for $LHTiO_2$ and anatase, respectively (Fig. 3B). These results qualitatively agree with multiple reports on the

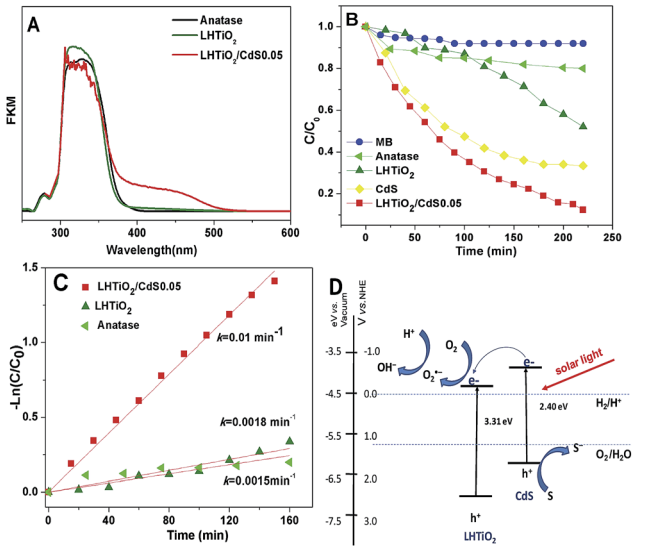

Fig. 3 UV-vis diffuse reflectance spectra of anatase, $LHTiO_2$ and $LHTiO_2$/CdS (A), plots of the degradation of MB solution under sunlight of anatase, $LHTiO_2$, CdS NPs and $LHTiO_2$/CdS0.05 (B), kinetic degradation of anatase, $LHTiO_2$ and $LHTiO_2$/CdS0.05 (C), schematic illustration the photocatalytic mechanism of $LHTiO_2$/CdS (D).

improved photocatalytic efficiency of nanostructured TiO_2 with the presence of CdS.[19–23]

The photocatalytic performance of $LHTiO_2$ and $LHTiO_2$/Cd under sunlight could be to some extent correlated with their absorption in the visible spectrum (Fig. 3A). However, the nature of these two phenomena is probably different. In the former, the creation of new electronic states could occur in the band gap of TiO_2, while in $LHTiO_2$/CdS, visible light absorption should preferably occur in CdS, due to its narrow band gap, *i.e.* through sensitization arising from the junction of both semiconductors. The shape of the MB spectrum recorded in the range 200–750 nm remained practically unaltered throughout the process and the formation of any organic subproduct was not detected, thus pointing to the mineralization of the dye (Fig. S10†). The XRD pattern of $LHTO_2$/CdS after one photocatalysis cycle (Fig. S11†) indicated that the composite retained its lamellar nature but lost some crystallinity.

A probable mechanism for the degradation of MB over $LHTiO_2$/CdS is schematically illustrated in Fig. 3D. During irradiation, the photoinduced charge carriers are primarily created on the CdS nanoparticle. The photoexcited electron on the CdS conduction band (CB) can be easily transferred to the CB of the TiO_2 nanosheet owing to suitable matching between the energy positions of the conduction bands of both semiconductors, *i.e.* about 0.5 eV. Electrons accumulated on the inorganic moiety of $LHTiO_2$ can activate adsorbed molecular oxygen, producing superoxide radicals ($O_2^{\bullet-}$). Further reduction of $O_2^{\bullet-}$ generates peroxide intermediates which decompose to hydroxyl radicals capable of accomplishing dye mineralization. The photogenerated holes stranded in the CdS cannot oxidize OH groups into hydroxyl radicals, but may instead oxidize the dye directly, or react with CdS itself (photocorrosion). However, the diminution in the photocatalytic efficiency of $LHTiO_2$/CdS with an excess of CdS (Fig. S9†), as well as the photocorrosion of the catalyst (Fig. S12†), indicates that the oxidation of MB by photo-holes is less important than that promoted by electrons on TiO_2.

To further understand the role of photogenerated radicals in MB degradation under sunlight, we carried out controlled experiments with the addition of either *tert*-butyl alcohol (TBA) or benzoquinone (BQ) as scavengers of hydroxyl radicals and $O_2^{\bullet-}$, respectively.[12,13,23] Only TBA slightly inhibited the photodegradation efficiency of $LHTiO_2$/CdS, corroborating a process mainly mediated by hydroxyl radicals. The low effect of the scavengers points to a protective effect of the organic surfactant, ensuring the oxidation process takes place at the TiO_2/carboxylic acid interface, far from the scavengers in the solution (Fig. S13†).

Conclusions

In summary, a new hybrid nanocomposite constituted of single TiO_2 nanosheets sandwiched between self-assembled long-chain carboxylic acid monolayers was prepared. The preliminary results show that this nanocomposite behaves as a semiconductor with photocatalytic activity in the degradation of methylene blue under sunlight with improved activity over anatase. This behaviour is attributed to the creation of discrete electronic levels inside the TiO_2 bandgap. The photocatalytic performance of the product can be further enhanced through its sensitization with CdS. The catalytic behaviour of the as-prepared nanocomposite as well its successful sensitization with CdS can be attributed to the absorbent ability of its organic component.

Acknowledgements

The authors acknowledge the Universidad Tecnologica Metropolitana, Universidad de Chile, FONDECT Grants 1151189 and 1131112, and CONICYT Grant FB0807 (CEDENNA). The authors would like to acknowledge Mr Roberto Villarroel by Raman Spectroscopy measurements.

Notes and references

1 H. J. Zhang, G. H. Chen and D. W. Bahnemann, *J. Mater. Chem.*, 2009, **19**, 5089–5121.
2 S. Hernández, D. Hidalgo, A. Sacco, A. Chiodoni, A. Lamberti, V. Cauda, E. Tresso and G. Saracco, *Phys. Chem. Chem. Phys.*, 2015, **17**, 7775–7786.
3 L. Yang, Y. Jiao, Z. Zhang, F. Qu, A. Umar and X. Wu, *ACS Appl. Mater. Interfaces*, 2014, **6**, 2174–2184.
4 D. Deng, S. Martin and S. Ramanathan, *Nanoscale*, 2010, **2**, 2685–2691.
5 R. Daghrir, P. Drogui and D. Robert, *Ind. Eng. Chem. Res.*, 2013, **52**, 3581–3599.
6 S. G. Kumar and L. G. Devi, *J. Phys. Chem. A*, 2011, **114**, 13211–13241.

7 N. Zhang, S. Liu, X. Fu and Y. Xu, *J. Phys. Chem. C*, 2011, **115**, 9136–9145.

8 S. B. Rawal, S. Bera, D. Lee, D. Jang and W. In Lee, *Catal. Sci. Technol.*, 2013, **3**, 1822–1830.

9 H. Xu, S. Ouyang, L. Liu, P. Reunchan, N. Umezawa and J. Ye, *J. Mater. Chem. A*, 2014, **2**, 12642–12661.

10 S. Mazumdar and A. Bhattacharyya, *RSC Adv.*, 2015, **5**, 34942.

11 C. Xue, T. Wang, G. Yang, B. Yang and S. Ding, *J. Mater. Chem. A*, 2014, **2**, 7674–7679.

12 J. Zhang, N. Zhang, Z. Tang and Y. Xu, *Chem. Sci.*, 2012, **3**, 2812–2822.

13 S. Liu, N. Zhang, Z. Tang and Y. Xu, *ACS Appl. Mater. Interfaces*, 2012, **4**, 6378–6385.

14 J. Luo, L. Ma, T. He, C. Ng, S. Wang, H. Sun and H. Fan, *J. Phys. Chem. C*, 2012, **116**, 11956–11963.

15 X. B. Chen, L. Liu, P. Y. Yu and S. S. Mao, *Science*, 2011, **331**, 746–750.

16 L. Xin and X. Liu, *RSC Adv.*, 2015, **5**, 71547–71550.

17 P. Chowdhury, J. Moreira, H. Gomaa and A. K. Ray, *Ind. Eng. Chem. Res.*, 2012, **51**, 4523–4532.

18 L. Wu, J. C. Yu and X. Fu, *J. Mol. Catal. A: Chem.*, 2006, **244**, 25–32.

19 Z. Chen and Y. Xu, *ACS Appl. Mater. Interfaces*, 2013, **5**, 13353–13363.

20 D. Baker and P. V. Kamat, *Adv. Funct. Mater.*, 2009, **19**, 805–811.

21 Y. Xie, G. Ali, S. Hwa Yoo and S. Oh Cho, *ACS Appl. Mater. Interfaces*, 2010, **2**, 2910–2914.

22 N. Qin, Y. Liu, W. Wu, L. Shen, X. Chen, Z. Li and L. Wu, *Langmuir*, 2015, **31**, 1203–1209.

23 J. Zhang, F. Xiao, G. Xiao and B. Liu, *New J. Chem.*, 2015, **39**, 279–286.

24 J. Zhao, T. Wu, K. Wu, K. Oikawa, H. Hidaka and N. Serpone, *Environ. Sci. Technol.*, 1998, **32**, 2394–2400.

25 H. N. Kim, T. W. Kim, I. Y. Kim and S. J. Hwang, *Adv. Funct. Mater.*, 2011, **21**, 3111–3118.

26 J. R. Jokisaari, D. Bayerl, K. Zhang, L. Xie, Y. Nie, D. G. Schlom, E. Kioupakis, G. W. Graham and X. Pan, *Chem. Mater.*, 2015, **27**, 7896–7902.

27 C. B. Mendive, D. W. Bahnemann and M. A. Blesa, *Catal. Today*, 2005, **101**, 237–244.

28 F. Urbach, *Phys. Rev.*, 1953, **92**, 1324.

29 H. Yaghoubi, Z. Li, Y. Chen, H. T. Ngo, V. R. Bhethanabotla, B. Joseph, S. Ma, R. Schlaf and A. Takshi, *ACS Catal.*, 2015, **5**, 327–335.